We are IntechOpen, the world's leading publisher of Open Access books Built by scientists, for scientists

4,800
Open access books available

122,000
International authors and editors

135M
Downloads

Our authors are among the

154
Countries delivered to

TOP 1%
most cited scientists

12.2%
Contributors from top 500 universities

CLARIVATE ANALYTICS BOOK CITATION INDEX INDEXED

WEB OF SCIENCE™

Selection of our books indexed in the Book Citation Index in Web of Science™ Core Collection (BKCI)

Interested in publishing with us?
Contact book.department@intechopen.com

Numbers displayed above are based on latest data collected.
For more information visit www.intechopen.com

Chapter 2

Steady State Thermal Analysis of a Tri-Wing Solar Chimney

R. S. Bello, C. N. Ezebuilo, T. A. Adegbulugbe and K. A. Eke

Additional information is available at the end of the chapter

http://dx.doi.org/10.5772/59721

1. Introduction

The solar chimney is one of the technologies which work on the principle of buoyancy, in which air is heated through the greenhouse effect generated by solar radiation (heat energy) at low cost. The solar chimney is a passive solar ventilation system (non-mechanical) that can be installed on roofs or in walls. The heat is transferred based on the convective cooling principle which works on the fact that hot air rises upward; these chimneys reduce unwanted heat during the day by displacing interior (warm) air with exterior (cool) air. Solar chimneys are mainly made of a black, hollow thermal mass with an opening at the top as an exit for the hot air. The air in the room exits from the top of the chimney (Figure 1). The process can also be reversed for room heating.

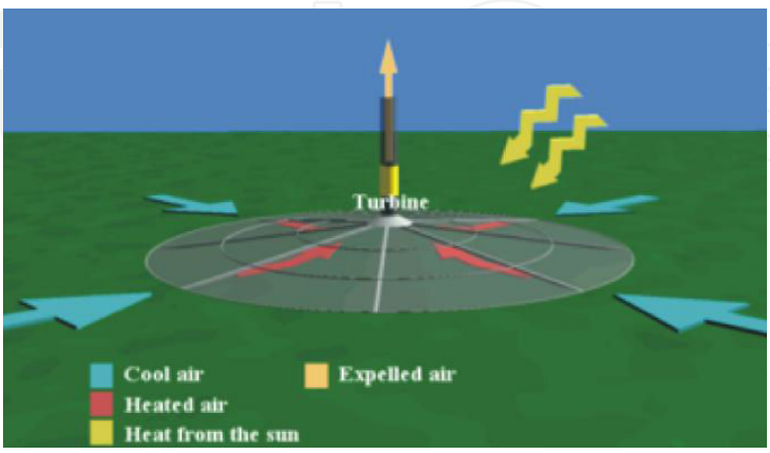

Figure 1. Solar chimney [1]

Solar chimney performance analysis for natural circulation dryers reported that simple air heater increases ventilation up to some extent but not sufficiently [1]. Also, Duffie, and Beckman, (2003) experimentally analyzed an inclined window-sized roof solar chimney and found its summer performance to increase. Duffie, and Beckman, (2003) equally studied the effects of various performance parameters like chimney width and height and solar radiation on flat-plate collectors. The thermal analysis on tri-wing collectors both at steady and transient states is an entirely new area of collector configuration research with limited research outcomes.

1.1. Project objective

For effective design of tri-wing solar chimney, solar parametric equations were utilized to model drying conditions at chimney inlet and outlet to maximize the differentials between system temperatures and air densities and their effects on drying applications. The air density depends on the temperature; hence, it also implies that the maximum differentials between the chimney air temperature and the ambient temp should give the best chimney performance.

The first mathematical model for the solar chimney design (Trombe wall) was given by [3, 16], and they also reported the concept of increasing airflow by increasing solar irradiation. This theoretical study also reported an air change per hour with change in the coefficient of fluid (air) discharge. Alter, (2011) reported the mathematical model of a conventional vertical chimney which operates under natural convention conditions where the temperature of the air inside the chimney is warmer than outside. Shiv et al., (2013) reported that solar chimney as a solar air heater may be represented by position (as vertical or horizontal chimney), or as a part of a wall (in the form of Trombe wall) or as a roof solar collector [6]. The roof solar chimney is the most convenient and mature technology used for buoyancy-driven natural ventilation systems [7, 8, 9].

A complete analysis of the tri-wing collector with a mathematical model is cumbersome because of its distinct features compared to an ordinary flat-plate model comparison of its performance effectiveness with experimental design data using high-precision apparatus and equipment offers a realistic solution. The objective of this study is to use analytical method to derive expressions for modelling drying effects of buoyant airflow created by solar heating of a tri-wing collector.

2. Experimental setup

The solar chimney used in modelling drying conditions is shown in Figure 2. The experimental solar chimney is a hollow cylindrical channel of glass glazing. The walls of the chimney were made as smooth as possible to reduce pressure losses due to wall friction. The absorbing surface (collector) is a tri-wing multi-flapped selective absorber plate draped inside the glazed glass. This chimney is mounted above the room space (drying chamber) through which dry air passes.

http://dx.doi.org/10.5772/59721

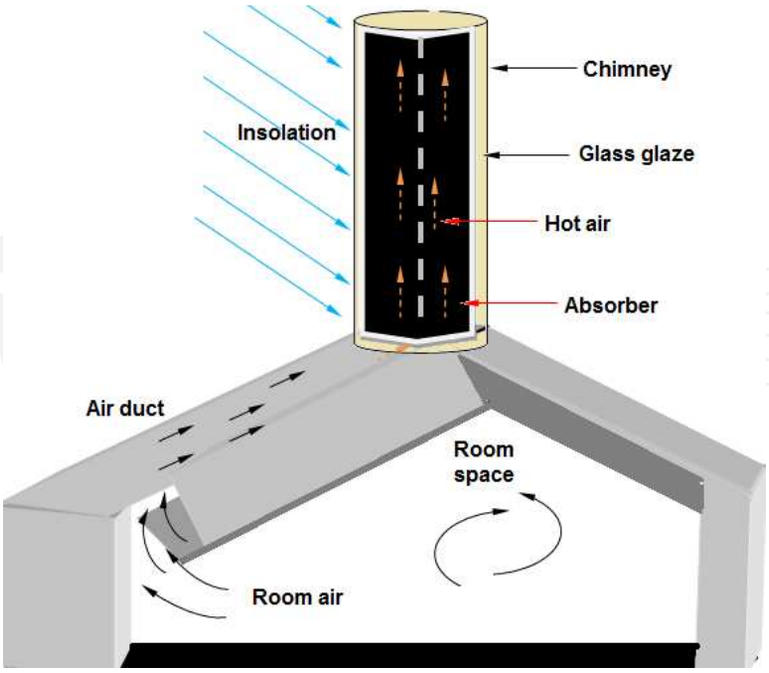

Figure 2. Schematic diagram of solar chimney

3. Solar incident radiation on each wing

The incident angle of radiation reaching any collector surface is expressed by the general expression

$$\text{Cos } \theta = -\sin \delta \cos\varphi \cos\gamma + \cos \delta \sin \varphi \cos\gamma \cos\omega + \cos \delta \sin\gamma \sin\omega \quad (1)$$

This expression was used to model the following equations for each of the wings in terms of ω as

$$\text{Cos } \theta = -\left(0.1761 + 0.053 \cos\omega + 0.81 \sin\omega\right) \text{ for wing1} \quad (2)$$

$$\text{Cos } \theta = -\left(0.353 + 0.1106 \cos\omega\right) \text{ for wing2} \quad (3)$$

$$\text{Cos } \theta = -\left(0.1764 - 0.053 \cos\omega - .1764 - 0.0\omega\right) \text{ for wing3} \quad (4)$$

Previously the expression for all the wings has been derived as

$$\text{Cos}\theta_z = 0.9288\text{Cos}\theta - .9288 \quad (5)$$

4. System heat transfer mechanism in the model

A complex differential analysis is required to fully analyze the multi-flapped collector due to shadows and the transient heat flow of flaps at different potentials (Figure 3). For instance, when the sun is between the azimuth of east and south, wings 1 and 2 receive full-area radiation at different incident angles, while wing 3 receives partial-area direct radiation due to the shadow of wing 2 cast on it. The case is reverse when the sun is between the azimuths of south and west, the critical time of changeover. When the sun is over the azimuth of 0°, wings 1 and 3 receive full-area direct radiation at different incident angles, and wing 2 receives partial direct radiation. This only happens intermittently (Figure 3).

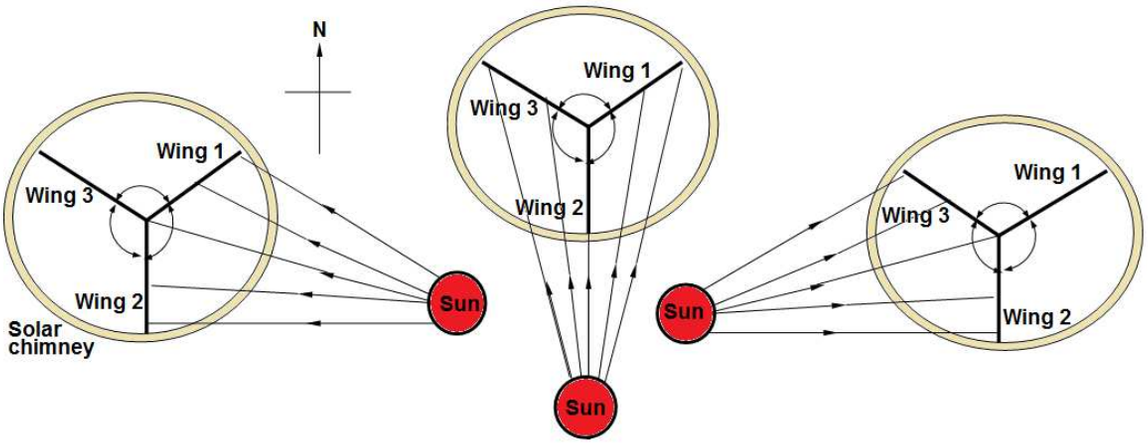

Figure 3. Azimuth positions of the solar insolation with respect to the three absorber surfaces

The analysis of a tri-axially configured surface is cumbersome because of its distinct features compared to an ordinary flat-plate model; to overcome this, an assumption is made that the collector absorber material is a highly conductive metal such that heat due to absorbed radiation is evenly distributed in all the flaps. This implies that solar radiation incident on the collector is such that there is no temperature gradient anywhere in the collector (i.e. the absorber is isothermal at any point in time).

4.1. Assumptions on analytical methods

In the course of analysis of this solar collector, a number of overriding assumptions were made which made the correlation of analyzed values comparable to experimental data values. Experimental data for this type of solar collector at the study location (Nsukka, Enugu state, Nigeria) was not available; however, such correlations provide a complete analytical method. Such assumptions considered a vertical tri-wing absorber collector heated by insolation to a temperature T_p with free convection boundary layer effects and also considered a zero air stream velocity which could be increased to some maximum value and then decreased to zero again due to free stream conditions, provided the gap between the plate and the cover is much greater than the boundary layer thickness.

http://dx.doi.org/10.5772/59721

To effectively model flow within the solar chimney, the analytical method employed required the following steps:

1. First, determination of available solar radiation data in the study location.
2. Second, evaluation of optical properties of glazing materials (assumed to be same as that of flat glazed collectors).
3. Third, consideration of the electrical analogy of the system (from which the collector efficiency factor F′ expression and the overall collector heat loss U_L expression were derived).
4. Last, the heat transfer analysis and collector performance.

4.2. Solar insolation data at experimental setup location

The experimental setup was located at Nsukka, Nigeria, longitude 7° 23′ 45″ E and latitude 6° 51′ 24″ N [10], and the data acquisition method was adopted from the works of [11]. Solar data of the year and declination of that day were taken. This data was used as a case study (data presented in another chapter of this book) with the assumption that insolation recorded for a particular month is approximately the same for the same month for every other year. Also obtained from the literature were the measurement of instantaneous values of total insolation I_T against diffuser I_d and beam I_b insolations. From the instantaneous values, an expression relating to the total and beam insolations was deduced by the method of least squares for a third-order polynomial that fits the distribution of data. The polynomial is deduced as

$$I_b = 0.01524I_T^3 - 0.0152I_T^2 + 0.988I_T - 0.9882\left(\frac{MJ}{m^2}\right) \text{for } I_T > 0.22\left(\frac{MJ}{m^2}\right) \tag{6}$$

And with linear regression of natural logarithm of data distribution,

$$I_b = e^{(1.761\ln I_T - 1.761}\left(\frac{KJ}{m^2}\right) \text{for } I_T > 220\left(\frac{KJ}{m^2}\right) \tag{7}$$

$$I_d = I_T - I_b \tag{8}$$

where I_T = total insolation, I_b = direct beam insolation and I_d = diffuse insolation.

These parameters were used to compute instantaneous values of hourly insolation for the day of the year when data were taken.

Solar radiation on a tilted collector is made up of the beam radiation component, the diffuse radiation component and the ground-reflected diffuse radiation components. Hence, the total hourly solar radiation on a tilted surface is the summation of the three components:

$$I_c = I_{bc} + I_{dc} + I_{dgc} \tag{9}$$

where subscript c denotes solar radiation on the collector. Furthermore,

$$I_c = I_{bc}R_b + I_d\left[(1+\cos\beta)/2\right] + \left(I_d + I_b\right)\rho\left[1/2\left(1-\cos\beta\right)\right] \tag{10}$$

For the case study, considering the collector being a vertical wall and no vegetation covering the ground, $\beta=90°$ and $\rho=0.2$. Substituting these conditions into the equation of the total hourly radiation on the collector gives

$$I_c = I_{bc}R_b + 0.5I_d + 0.1\left(I_d + I_b\right)\left(R_b + 0.1\right)I_b + 0.6I_d \tag{11}$$

Both sides of each wing are exposed to diffuse radiation, while only one side of the wings is exposed to direct beam radiation depending on the area factor receiving this direct radiation. Hence, the total radiation aimed at each wing of the collector is

$$I_{ci} = \forall I_b R_{bi} + 2\left[0.5I_d + 0.1\left(I_d + I_b\right)\right] = \left(\forall R_b + 0.2\right)I_b + 1.2I_d \tag{12}$$

Thus, the total radiation aimed at the whole collector in the chimney is

$$I_c = I_{c1} + I_{c2} + I_{c3} \tag{13}$$

Numbered subscripts 1, 2 and 3 denote wing positions.

5. Optical properties of glazing and absorption of solar radiation

The determination of collector performance requires the evaluation of the amount of solar radiation actually absorbed by the collector through glazing. Optical properties (transmittance, reflectance and absorptance) of the glaze cover, affects the absorption of solar radiation. These optical properties depend on the thickness of glazing and the refractive index and extinction coefficient of the glaze material. At a particular zenith angle of the sun, there are different incident angles of radiation on the circumference of the cylindrical glazing of the collector, unlike the flat-plate collector which has one uniform incident angle of radiation throughout the surface of glaze. Due to this feature, the evaluation of optical properties of a cylindrical glaze is complex. Though the glaze is cylindrical, the absorber plate is flat; hence, it was assumed that optical properties of a flat glass glazing are approximate to that of a cylindrical glass glazing. According to [12], expressions for reflection of unpolarized radiation passing from a medium with refractive index n_1 to another with refractive index n_2 are

http://dx.doi.org/10.5772/59721

$$r_r = \frac{\sin^2(\theta_2 - \theta_1)}{\sin^2(\theta + \theta_1)} \text{and } r_1 = \frac{\tan^2(\theta_2 - \theta_1)}{\tan^2(\theta_2 + \theta_1)} \tag{14}$$

where θ_1 and θ_2 are the angles of incidence and refraction. The average of reflectance of unpolarized radiation [12] is then

$$r = 0.5(r_\perp + r_\parallel) \tag{15}$$

where $r_\perp$. and $r_\parallel$ represents perpendicular and parallel reflectance components of the unpolarized radiation. The angle of refraction, θ_2, is related to the refractive indices and the incident angle by Snell's law expressed as

$$\theta_2 = \sin^{-i}\left[\frac{n_1}{n_2(\sin\theta_1)}\right] \tag{16}$$

For air, n_1 is approximately equal to 1. Consequently, the expressions for transmission of unpolarized radiation passing through a slab of glass from one interface to another interface and neglecting absorption decomposed to perpendicular and parallel components are as follows:

For a perpendicular component,

$$\tau_\perp = \left[\frac{1-\tau_\perp}{1+\tau_\perp}\right] \tag{17}$$

For a parallel component,

$$\tau_\parallel = \left[\frac{1-\tau_\parallel}{1+\tau_\parallel}\right] \tag{18}$$

where $\tau_\perp$ and $\tau_\parallel$ represent the perpendicular component and the parallel component of transmittance of unpolarized radiation for single cover glaze.

The average transmittance of these two components is

$$\tau_r = \frac{\left(\tau_\perp + \tau_\parallel\right)}{2} \tag{19}$$

In order to account for absorption, a loss factor was introduced by Bourguer's law:

$$\tau_2 = e^{-[kL/cos\theta_2]} \tag{20}$$

where k is the extinction coefficient (which varies from $4m^{-1}$ for white glass to $32m^{-1}$ for green glass). L is the thickness of the glass. In this study, the thickness of cover glass was taken to be 2.5mm, the extinction coefficient $5m^{-1}$ and the refractive index 1.526. The product k.L = 0.0025m x $5m^{-1}$ = 0.0125.

Some of the radiation passing through the glaze and striking the absorber plate is reflected back to the cover system. However, not all of this radiation is lost, since some of it is reflected back to the plate. The multiple reflections and absorptions between the plate and the cover is the greenhouse effect. To account for this greenhouse phenomenon, the actual fraction of incident radiation absorbed by the plate is called the transmittance-absorptance product, ($\tau\alpha$). tThis is reasonably approximated as

$$\left(\tau\alpha\right) = \mathrm{A}\left(\tau\right)\alpha_\mathrm{p} \tag{21}$$

The constant A ranges from 1.01 to 1.02, but for conservativeness, 1.01 is preferred:

$$\left(\tau\alpha\right) = 1.01\left(\tau\right)\alpha_\mathrm{p} \tag{22}$$

For transmittance of diffuse radiation, the effective incident angle θ_1 for vertical collectors is 59.5° for both ground and sky diffuse radiation. Hence, the effective refractive angle θ_2 of diffuse radiation from Snell's law is

$$\theta_2 = \sin^{-i}\left[\frac{n_1}{n_2}\left(\sin\theta_1\right)\right] \tag{23}$$

Likewise, the reflection components are

$$r_\perp = \frac{\sin^2(\theta_2 - \theta_1)}{\sin^2\left(\theta_2 + \theta_1\right)} \tag{24}$$

$$r_\parallel = \frac{\tan^2(\theta_2 - \theta_1)}{\tan^2(\theta_2 + \theta_1)} \tag{25}$$

The transmittance components are

$$\tau_{\perp} = \frac{\left(1-\tau_{\perp}\right)}{\left(1+\tau_{\perp}\right)} \tag{26}$$

$$\tau_{\parallel} = \frac{\left(1-\tau_{\parallel}\right)}{\left(1+\tau_{\parallel}\right)} \tag{27}$$

Cover absorptance τ_a was evaluated with the relation

$$\tau_a = e^{-\text{was ev}\theta_2} \tag{28}$$

Hence, the resultant transmittance for diffuse radiation is

$$\tau_d = \tau_r.\tau_a \tag{29}$$

Since all necessary optical properties of the glass glazing have been evaluated, the amount of solar radiation actually absorbed by the collector can be easily deduced. The total incident radiation aimed at each wing of the collector is

$$I_{ci} = \forall I_b R_{bi} + 2\left[0.5I_d + 0.1\left(I_d + I_b\right)\right] \tag{30}$$

the total absorbed solar radiation of each wing is

$$S_i = (\tau\alpha)_b \forall I_b R_{bi} + 2(\tau\alpha)_b\left[0.5I_d + 0.1\left(I_d + I_b\right)\right] \tag{31}$$

$$= (\tau\alpha)_b \forall I_b R_{bi} + (\tau\alpha)_b\left[I_d + 0.2\left(I_d + I_b\right)\right] \tag{32}$$

The mean absorbed solar radiation, S, of the whole collector plate is evaluated by the relation

$$S = 1/3\left[S_1 + S_2 + S_3\right] \tag{33}$$

6. The collector efficiency factor and the collector loss coefficient

Considering the unusual configuration of the tri-wing absorber plate, a section of it was reduced to a vertical flat-plate collector over both sides of the plate without back insulation. This implies that a wing of the absorber can be treated as a flat-plate air heater with flow over both sides of the plate. The determination of the collector efficiency factor F′ and the collector loss coefficient U_L provided the basis for the analytical prediction of collector performance when used in the Hottel-Whillier-Bliss equation [12, 13]:

$$q_u = F^{'}\left[S - U_l\left(T_r - T_a\right)\right] \tag{34}$$

The collector efficiency factor $F^{'}$ is defined as the ratio of the actual useful energy gain to the useful gain that would result if the collector absorbing surface had been at the local fluid temperature, that is

$$F^{'} = \frac{q_u}{\left[S - U_l\left(T_r - T_a\right)\right]} \tag{35}$$

where q_u is the actual useful heat collector rate, S is absorbed radiation and T_r is average fluid temperature.

The collector loss coefficient U_l is defined as the lumped overall heat loss value of the whole collector to the operating temperature difference of the collector, that is

$$U_l = E_{loss}(T_p - T_a) \tag{36}$$

where E_{loss}= heat loss, T_p= absorber plate temperature and T_a= ambient temperature of surrounding air.

To conform to the performance equation of a flat-plate collector, the configuration of the chimney collector is transformed to suit the equation. Criteria for the transformation are as follows:

1. The total area of the tri-wing absorber plate is equal to the total area of the flat absorber plate.
2. The height of the chimney collector is the same as the height of the resulting flat absorber plate.
3. The area of the circular inlet column of the chimney collector and the rectangular area inlet column of the resulting flat-plate collector are equal throughout the height of the collector.

http://dx.doi.org/10.5772/59721

4. The resulting flat-plate absorber is positioned within the rectangular column such that the flow is halved.

5. Size difference of the glass glazing of the two cases is neglected. The resulting flat-plate collector has an absorber plate 5.3m in height and 2.4m in breadth enclosed by a rectangular channel of glass glazing measuring 2.46m by 0.8587m in length and breadth. Thus, the flow width on either side of the plate is about 43cm.

6.1. Electrical analogy

According to [12], the usual procedure of deriving F' and U_l is by converting a schematic diagram of the collector system to a thermal network of electrical analogy and analyzing the resulting circuit. A schematic diagram with equivalent thermal network is shown in Figure 4.

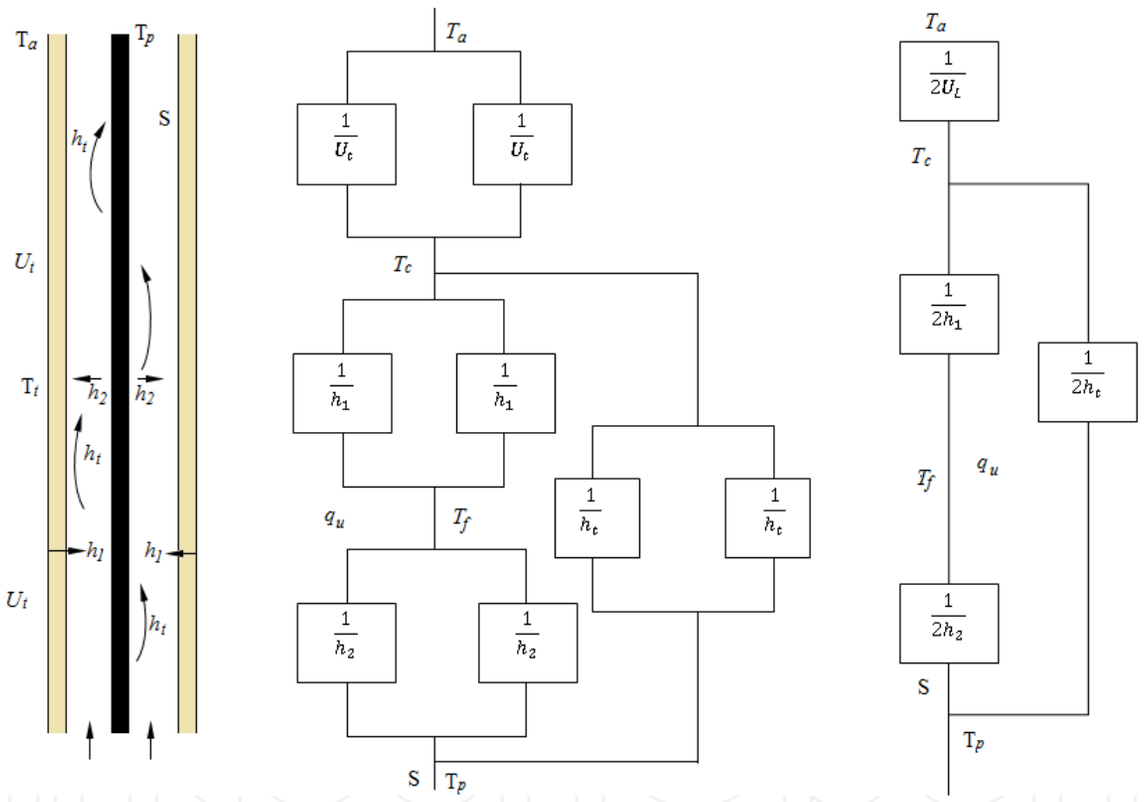

Figure 4. Schematic diagram with equivalent thermal network

At the leading edge of the flat absorber plate, airflow is halved to flow on both sides of the plate. Absorbed solar energy heats up the plates to a temperature T_p, and energy is transferred to fluid at temperature T_r through the convection heat transfer coefficient h_2 and to the cover glass through the linearized radiation heat transfer coefficient h_1. Energy is also transferred to the cover glass from the fluid though the convective heat transfer coefficient h_t, and finally energy is lost to the ambient air through the combined convection and radiation coefficient U_t from the cover glass.

7. Energy balance equations

Energy balance equations on the cover, the plates and the fluid are derived as follows:

$$2U_t\left(T_a - T_c\right) + 2h_1\left(T_p - T_c\right) + 2h_2\left(T_r - T_c\right) = 0 \tag{37}$$

$$S + 2h_1\left(T_c - T_p\right) + 2h_2\left(T_r - T_p\right) = 0 \tag{38}$$

$$2h_1\left(T_c - T_r\right) + 2h_2\left(T_p - T_r\right) = q_u \tag{39}$$

Simplifying and expanding the expressions as a function of heat transfer coefficients and temperatures yields

$$U_tT_a - U_tT_c + h_rT_p - h_rT_c + h_1T_r - h_1T_c = 0 \tag{40}$$

$$0.5S + h_1T_c - h_1T_p + h_2T_r - h_2T_p = 0 \tag{41}$$

Equations (40) and (41) can be expressed as

$$A = BT_c - = T_p \tag{42}$$

$$D = ET_p - = T_c \tag{43}$$

where $A = U_tT_a + h_1T_r$, $B = U_t + h_r + h_1$, $C = h_r$, $D = 0.5S + h_2T_r$ and $E = h_r + h_2$.

Solving equations (42) and (43) simultaneously and re-substituting values into equations (40) and (41),

$$T_p = \frac{AC + BD}{\left[BE - C^2\right]} = \frac{(U_tT_a + h_1T_r)h_r + \left(U_t + h_r + h_1\right)0.5S + h_2T_r}{(U_t + h_r + h_1)(h_r + h_2) - {h_r}^2} \tag{44}$$

$$T_p = \frac{AE + CD}{\left[BE - C^2\right]} = \frac{(U_tT_a + h_1T_r)(h_r + h_2) + (0.5S + h_2T_r)h_r}{(U_t + h_r + h_1)(h_r + h_2) - {h_r}^2} \tag{45}$$

http://dx.doi.org/10.5772/59721

Subtracting T_r from both sides of equations (44) and (45),

$$T_p - T_r = \frac{U_t h_r \left(T_a - T_r\right) + 0.5S\left(U_t + h_r + h_1\right)}{\left(U_t + h_r + h_1\right)\left(h_r + h_2\right) - h_r^{\,2}} \tag{46}$$

$$T_c - T_r = \frac{\left(U_t h_r + U_t h_2\right)\left(T_a - T_r\right) + 0.5Sh_r}{\left(U_t + h_r + h_1\right)\left(h_r + h_2\right) - h_r^{\,2}} \tag{47}$$

Substituting equations (46) and (47) into equation (39),

$$0.5q_u = \frac{0.5S\left(h_1h_r + U_th_2 + h_rh_2 + h_1h_2\right) + U_t\left(h_1h_r + h_rh_2 + h_1h_2\right) + \left(T_a - T_r\right)}{\left(U_t + h_r + h_1\right)\left(h_r + h_2\right) - h_r^{\,2}} \tag{48}$$

Rearranging equation (46),

$$q_u = \frac{S\left(h_1h_r + U_th_2 + h_rh_2 + h_1h_2\right)}{\left(U_t + h_r + h_1\right)\left(h_r + h_2\right) - h_r^{\,2}} - \frac{2U_t\left(h_1h_r + h_rh_2 + h_1h_2\right) + \left(T_a - T_r\right)}{\left(U_t + h_r + h_1\right)\left(h_r + h_2\right) - h_r^{\,2}} \tag{49}$$

Comparing equation (49) with the Hottel-Whillier-Bliss equation, $q_u = F'[S - U_L(T_r - T_a)]$, it can be deduced that

$$F' = \frac{h_1h_r + U_th_2 + h_rh_2 + h_1h_2}{\left(U_t + h_r + h_1\right)\left(h_r + h_2\right) - h_r^{\,2}} \tag{50}$$

$$U_L = \frac{2U_t\left(h_1h_r + h_rh_2 + h_1h_2\right) + \left(T_a - T_r\right)}{\left(h_1h_r + U_th_r + h_rh_2\right) + h_1h_2} \tag{51}$$

It has been demonstrated experimentally that $h_1 = h_2 = h$ according to Duffie and Beckman; therefore, equations (47) and (48) reduce to

$$F' = \frac{h\left(U_t + 2h_r + h\right)}{\left(U_t + h_r + h_1\right)\left(h_r + h_2\right) - h_r^{\,2}} \text{ and } U_L = \frac{2U_t\left(2h_r + h\right) + \left(T_a - T_r\right)}{\left(U_t + 2h_r\right) + h} \tag{52}$$

It is necessary to outline expressions of heat coefficients as functions of F' and U_L. These heat coefficients are expressed as

$$U_t = \left(h_{wind} + h_{rea}\right) \tag{53}$$

where h_{rea} is the radiative loss coefficient between the cover and ambient air expressed as

$$h_{rea} = \varepsilon_c \alpha \left(T_c^2 + T_s^2\right)\left(T_c - T_s\right) \tag{54}$$

where glass cover emittance ε_c=0.88, Stefan-Boltzmann constant $\alpha = 5.6 \times 10^{-1} w/m^2k^4$ and sky temperature $T_s = 0.0552T_a^{1.5}$.

The convective atmospheric heat loss coefficient due to wind, h_{wind}, is dependent on the prevailing wind velocity given by [14] as

$$h_{wind} = 5.8 + 3.8v \tag{55}$$

where v (ms^{-1}) is the wind velocity (2 ms^{-1}) for the study location); thus,

$$h_{wind,\ location} = 5.8 + 3.8x2 = 13.4\ w/m^2{}^\circ c \tag{56}$$

The radiative heat loss coefficient between the plate and the cover after linearization is given as

$$h_r = \frac{\sigma}{\left(\varepsilon_c^{-h} + \varepsilon_p^{-h} - h\right)\left(T_c^2 + T_p^2\right)\left(T_c - T_p\right)} \tag{57}$$

where absorber plate emittance $\varepsilon_p = 1 - \alpha_p = 0.1$.

8. Heat transfer and collector performance analysis

A review of the principles and theories governing natural free convection heat transfer [4] is done for the determination of other collector performance parameters. Thus, considering a vertical absorber plate of one wing of the collector heated by insolation to a temperature T_p, a free convection boundary layer is formed. The boundary layer is such that at the wall of the plate, the velocity of air stream is zero. This increases to some maximum value and then

http://dx.doi.org/10.5772/59721

decreases to zero due to free stream conditions, provided the gap between the plate and the cover is much greater than the boundary layer thickness. The equation of motion for such a system is derived from the Navier-Stokes momentum equation of fluid flow given by [15]:

$$\varrho\left(\frac{\partial u}{\partial x}+v\frac{\partial u}{\partial y}\right)=-\varrho g+\frac{\mu\partial^2 u}{\partial y^2} \tag{58}$$

where ϱ is the density of air; x is the displacement in the vertical direction, the direction of buoyant flow; y is the displacement perpendicular to the direction of buoyant flow; U is the velocity component in the x -direction; v is the velocity component in the y-direction; p is air pressure; μ is the dynamic viscosity of air and g is acceleration due to gravity of value 9.18 (ms^{-2}).

Equation (58) can be expressed as

$$\left(U\frac{\partial u}{\partial x}+v\frac{\partial u}{\partial y}\right)=\frac{\partial p}{\partial x}-\rho g+\mu\frac{\partial^2 u}{\partial y^2} \tag{59}$$

where $\frac{\partial p}{\partial x}=g.\,\varrho_\infty$ and ϱ_∞ is the free stream air density.

The density difference can be expressed in terms of the volume coefficient of expansion, β, defined by

$$=\frac{1}{V}\left(\frac{\partial V}{\partial T}\right)_p=\frac{1}{V_\infty}\left[\frac{V-V_\infty}{T-T_\infty}\right]=\left[\frac{\rho-\rho_\infty}{T-T_\infty}\right] \tag{60}$$

Substituting equation (59) into (58) brings the momentum equation to

$$\varrho\left(U\frac{\partial u}{\partial x}+V\frac{\partial u}{\partial y}\right)=\varrho g\beta\left(T-T_\infty\right)+\mu\frac{\partial^2 u}{\partial y^2} \tag{61}$$

integrating equation (61) with respect to y from the boundary layer thickness δ to the plate surface; since the velocity in the flow direction u is much greater than the velocity component perpendicular to the flow direction v, hence v tends to zero compared to u. The integral momentum equation becomes

$$\frac{d}{dx}\left[\int_0^\delta \varrho u^2 dy\right]=\int_0^\delta \varrho\beta g\left(T-T_\infty\right)dy-\mu\frac{\partial u}{\partial y}=0 \tag{62}$$

The functional relation between the temperature distribution and the boundary layer thickness is needed to solve equation (61). From the prevailing conditions of the system, temperature $T=T_p$ at $y=0$, $T=T_\infty$ at $y=\delta$ and $\frac{dt}{dy}=0$ at $y=\delta$, a parabolic temperature function can be assumed to represent the temperature profile of the system with respect to y.

Therefore, let the function be of the form

$$T = Ay^2 + By + C \tag{63}$$

Substituting the conditions of flow into equation (61) gives

$$T - T_p = Ay^2 - An\delta y \text{ and } T_p - T_\infty = 2A\delta^2 - 2\delta^2 = A\delta^2 \tag{64}$$

Also the expression for the velocity profile is necessary to solve the integral momentum equation which can be deduced from the following flow conditions: $u=0$ at $y=0$, $u=0$ at $y=\delta$ and $\frac{\partial^2 u}{\partial y^2} = -\beta g(T-T_\infty)\big/ v$ at $y=0$. These four flow conditions can be fitted into a cubic equation of the form

$$\frac{u}{u_x} = Ay^3 + By^2 + Cy + D \tag{65}$$

where u_x is a fictitious velocity which is a function of displacement in the x-direction. Applying the conditions of flow into the cubic equation gives

$$\left.\begin{aligned} D &= 0, \\ C &= \left[\frac{\beta g\left(T_p - T_\infty\right)\delta}{4v}\right], \\ B &= \left[-\frac{\beta g\left(T_p - T_\infty\right)}{2v}\right], \\ A &= \left[-\frac{\beta\beta g\left(T_p - T_\infty\right)}{4v\delta}\right] \end{aligned}\right\} \tag{66}$$

http://dx.doi.org/10.5772/59721

Substituting these expressions into equation (65) and evaluating yields

$$\frac{u}{u_x} = \frac{\left[\frac{\beta g \delta^2 \left(T_p - T_\infty\right)}{4u_x v}\right] y}{\left(1 - \frac{y}{\delta}\right)^2} \tag{67}$$

The terms involving $(T_p - T_\infty)$, δ^2 and u_x may be incorporated into the function u_x so that the velocity profile can be reduced to

$$\frac{u}{u_x} = \frac{y/\delta}{\left(1 - \frac{y}{\delta}\right)^2} \tag{68}$$

Now the momentum equation of equation (61) when solved has its terms reduced to

$$\begin{aligned} \int_0^\delta : u^2 dy &= \int_0^\delta \frac{{u_x}^2}{\delta^2}\left[(y^2 - \frac{4y^3}{\delta} + \frac{6y^4}{\delta^2} - \frac{4y^5}{\delta^3} + \frac{y^6}{\delta^4}\right] dy \\ &= \frac{{u_x}^2}{\delta^2}\left(\frac{y^3}{3} - \frac{y^4}{\delta} + \frac{\frac{6}{5y^6}}{\delta^3} + \frac{y^7}{\delta^4}\right) y_o^\delta \\ &= {u_x}^2 \delta(\frac{1}{3} - \ = \frac{6}{5} - \frac{2}{3} + \frac{1}{7}) \end{aligned} \tag{69}$$

$$\Rightarrow \int_0^\delta : u^2 dy = \frac{{u_x}^2 \delta}{1.05} \tag{70}$$

Solving equation (69) in terms of temperature variables,

$$\int_0^\delta : \left(T - T_\infty\right) dy = \int_0^\delta : \left(T_p - T_\infty\right)\left(1 - \frac{2y}{\delta} + \frac{y^3}{\delta^2}\right)_0^\delta = \left(T_p - T_\infty\right)\delta(1 - 1 + \frac{1}{3}) \tag{71}$$

$$\Rightarrow \int_0^\delta : \left(T - T_\infty\right) dy = \frac{1}{3}\left(T_p - T_\infty\right)\delta \tag{72}$$

$$\frac{\delta u}{\delta y}|_{y=0} = \frac{Ux}{\delta}\left(y - \frac{2y^2}{\delta} + \frac{y^3}{\delta^2}\right)|_{y=0} = \frac{Ux}{\delta}\left(1 - \frac{4y}{\delta} + \frac{3y^2}{\delta^2}\right)|_{y=0}$$
$$\Rightarrow \frac{\delta u}{\delta y}|_{y=0} = \frac{Ux}{\delta} \tag{73}$$

Substituting equations (67), (68) and (70) into equation (61),

$$\frac{1}{1.05}\left(\frac{d}{dx}u_x^{\,2}\right) = \frac{1}{3}g\beta\left(T_p - T_\infty\right)\delta - \frac{vx}{\delta} \tag{74}$$

where $v = \frac{\mu}{\varrho}$ is known as kinematic viscosity.

The energy equation for free convection of the collector system is expressed as

$$\varrho C_p\left(\frac{U\partial T}{\partial x} + V\frac{U\partial T}{\partial y}\right) = k\frac{\partial^2 T}{\partial y^2}, \text{ or } \left(\frac{U\partial T}{\partial x} + V\frac{U\partial T}{\partial y}\right) = \alpha\frac{\partial^2 T}{\partial y^2} \tag{75}$$

where $\alpha = \frac{k}{\varrho C_p}$ is called the thermal diffusivity. The integral form of equation (72) with velocity tending to zero is

$$\frac{d}{dx}\int_0^\delta : U\left(T - T_\infty\right)dy = \alpha\left.\frac{dT}{dy}\right|_y = 0 \tag{76}$$

From equation (67), it can be deduced that the relation of the order of magnitude between u_x and δ is $u_x - \delta^2$. Inserting this relation into equation (68) and solving yields $\delta - x^{1/2}$. Hence, it can be assumed that

$$u_x = Ax^{1/2} \text{ and } \delta = Bx^{1/4} \tag{77}$$

Introducing these expressions into equations (67) and (74) yields

$$\frac{5}{240}A^2Bx^{1/4} = g\beta\left(T - T_\infty\right)\left(\frac{Bx^{1/4}}{3}\right) - \left(\frac{A}{B}\right)vx^{1/4} \tag{78}$$

Solving for A and B in the above equation,

http://dx.doi.org/10.5772/59721

$$A = 5.17v\left(0.952 + Pr\right)^{-.95}\left[g\beta\left(T - T_{\infty}\right)\frac{x^3}{v^2}\right]^{-x95}\left[Pr\right]^{-r95} \tag{79}$$

$$B = 3.93Pr^{-\frac{1}{4}}\left[g\beta\left(T - T_{\infty}\right)\frac{x^3}{v^2}\right]^{-x3.}\left[Pr\right]^{-r3.} \tag{80}$$

Substituting the expression for A into equation (77) gives the fictitious velocity u_x at any point x as

$$u_x = 5.17v\left(0.952 + Pr\right)^{-\frac{1}{2}}\left(Gr_x\right)^{-r} \tag{81}$$

where Gr_x is the Grashof number at point x, this is given by

$$Gr_x = g\beta\left(T - T_{\infty}\right)\frac{x^3}{v^2} \tag{82}$$

The resultant expression for boundary layer thickness from equation (75) is

$$\frac{\delta}{x} = Bx^{-Be} = 3.93Pr^{-\frac{1}{2}}\left(0.952 + Pr\right)^{\frac{1}{4}}\left(Gr_x\right)^{-\frac{1}{4}} \tag{83}$$

The heat transfer coefficient may be evaluated using equation (62)

$$q_p = -kA\frac{dT}{dy} = kA\left(\frac{2}{\delta}\right)\left(T_p - T_{\infty}\right) = hA\left(T_p - T_{\infty}\right) \tag{84}$$

where it was derived that $h=\frac{2k}{\delta}$. Hence, the dimensionless equation for the heat transfer coefficient becomes the expression for Nusselt number Nu_x :

$$Nu_x = 0.508Pr^{-\frac{1}{2}}\left(0.952 + Pr\right)^{-\frac{1}{4}}\left(Gr_x\right)^{-\frac{1}{4}} \tag{85}$$

In the case study, it was assumed that solar heating of the collector is one of the constant heat flux conditions. In such a case, a modified Grashof number is introduced:

$$Gr_x^* = Gr_x.Nu_x = \frac{g\beta\, x^4 q_p}{kv^2} \tag{86}$$

where q_p is the plate heat flux. The local heat transfer coefficient is correlated as

$$Nu_x = \frac{hx}{k} = 0.6\left(Gr_x Pr\right)^{0.2},\ 10^5 < Gr_x^* < 10^{11}, q_p = \text{constant} \tag{87}$$

For the turbulent range, the average heat transfer coefficient for the constant heat flux cause is obtained from

$$h = \frac{1}{L}\int_0^1 h_x d_x = 1.25h_x \tag{88}$$

It has been established that during distribution the local heat transfer coefficient is essentially with x when turbulent free convection is encountered. In such a case, the average heat transfer coefficient is $h=h_x$. The mean velocity of air stream due to natural convection was obtained from evaluating the mean value of velocity distribution of equation (64) as

$$u = u_x\int_0^1\left[\frac{y}{\delta}\left(1-\frac{y}{\delta}\right)\right]d\left(\frac{y}{\delta}\right) = 0.0833U_x \tag{89}$$

The volumetric flow rate is

$$V_o = C_d A_o U \tag{90}$$

The coefficient of discharge C_d is taken as 0.6 as adapted from [1]. Then the mass flow rate is obtained from the expression

$$\dot{m} = \rho V_o \tag{91}$$

In the previous section, expressions for the overall collector heat loss coefficient U_L and the collector efficiency factor F', which are very important performance parameters, were derived. These parameters are applied in the evaluation of useful energy rate extracted from the collector. To incorporate the flow rate and express the system energy equation using the collector inlet temperature, another performance parameter is introduced as the collector heat removal factor. The collector heat removal factor F_R is defined as the ratio of actual useful heat

http://dx.doi.org/10.5772/59721

collector rate to useful heat collector rate attainable with the entire collector surface at the inlet fluid temperature. This is stated mathematically as

$$F_R = \frac{mC_p\left(T_o - T_1\right)}{A_c\left[S - U_L\left(T_1 - T_a\right)\right]} = \left[\frac{mC_p}{A_c U_L}\right]\left[1 - e^{-\frac{A_c U_L F}{mC_p}}\right] \tag{92}$$

Thus, the energy equation of the system becomes

$$Q_u = 2A_c F_R\left[S - U_L\left(T_1 - T_a\right)\right] \tag{93}$$

The efficiency of the whole collector system η defined as the ratio of the useful heat extracted from the collector Q_u to the total incident solar radiation on the collector is mathematically expressed as

$$\eta = \frac{Q_u}{A_c I_T} = 2F_R\left[\left(\tau\alpha\right)_c - \frac{U_L}{I_T}\left(T_1 - T_a\right)\right] \tag{94}$$

where $(\tau\alpha)$ is the effective transmittance-absorptance product of the collector glazing,

$$\left(\tau\alpha\right)_c = \frac{S_T}{I_T} \tag{95}$$

where temperatures T_1 and T_a are the collector's inlet and outlet temperatures, respectively.

9. Results and discussions

The modelled parameters from the analysis of the momentum equation provide a platform to analyze the thermal behaviour on each wing based on the use of a selective surface. This was used to graphically illustrate the heat flow pattern in the chimney and the radiative effects on the emitting and receiving surfaces. At any position of the sun, only two wings of the collector receive full-area direct radiation. At a smaller zenith angle, a larger portion of the farthest wing is lightened, while a smaller portion is lightened at a higher zenith angle. Figure 5 gives the direct beam area ratio ∀ for the three wings of the collector with respect to midpoint solar time.

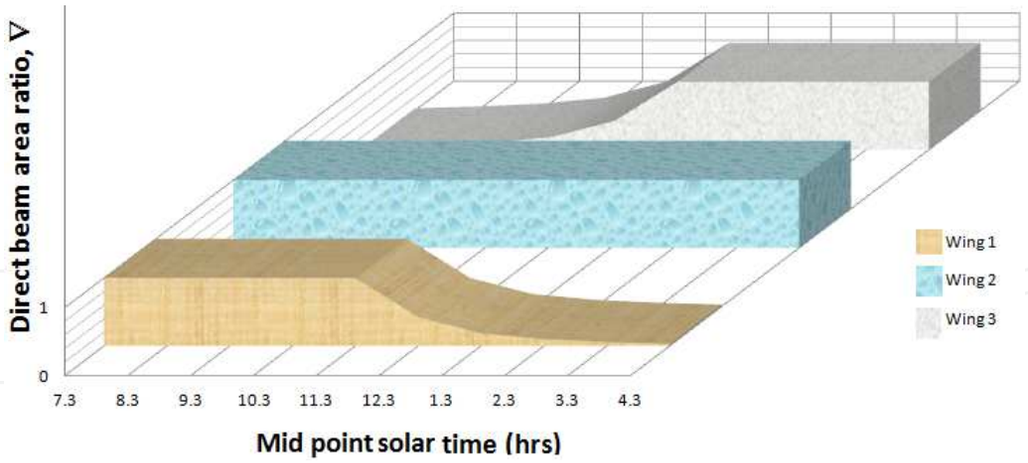

Figure 5. Direct beam area ratio ∀ for the three wings

The shading of the wings was taken into account to evaluate the actual direct beam radiation absorbed by each wing so that the average radiation absorbed by the whole collector can be deduced. To investigate the shape of the lightened area of a wing at any time interval, the zenith angle and the hour angle are required. The shape of the lightened region of the shadowed wing is always triangular depending on the zenith angle of the sun. Five variants of the shadowed wing model are shown in Figure 6.

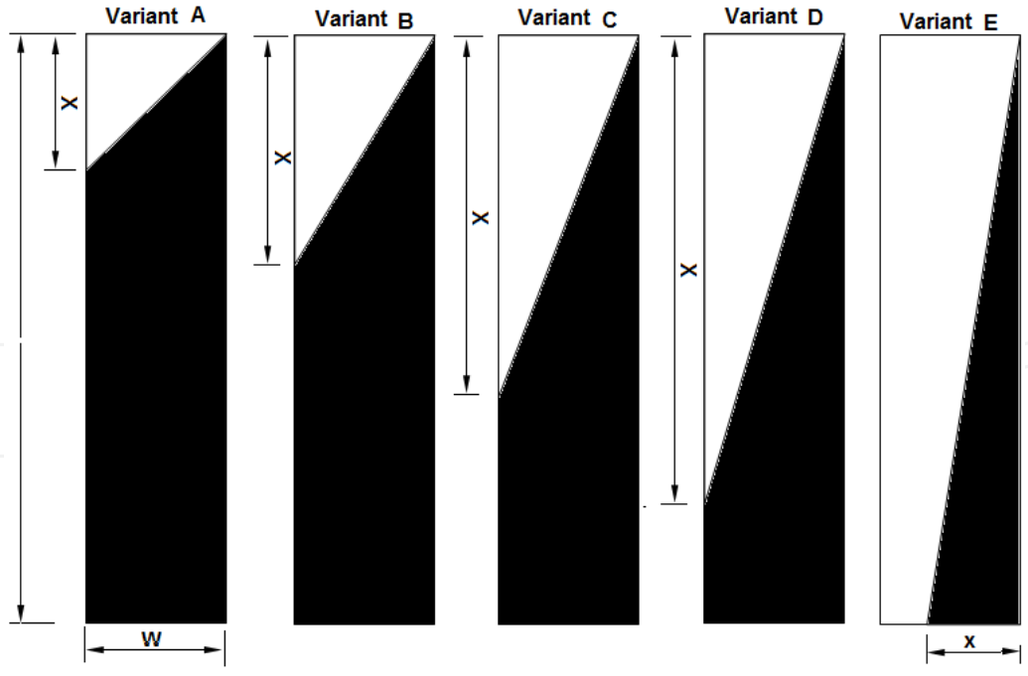

Figure 6. Variants of the shadowed wing model

Figure 7 shows the graph of temperature elevation and mass flow rate and insolation which points out that increase in temperature elevation is not always consequent on increase in the

http://dx.doi.org/10.5772/59721

mass flow rate as illustrated by the negative gradient of mass flow rate between 11.30 am and 1.30 pm compared to the positive gradient of temperature elevation within the same insolation range.

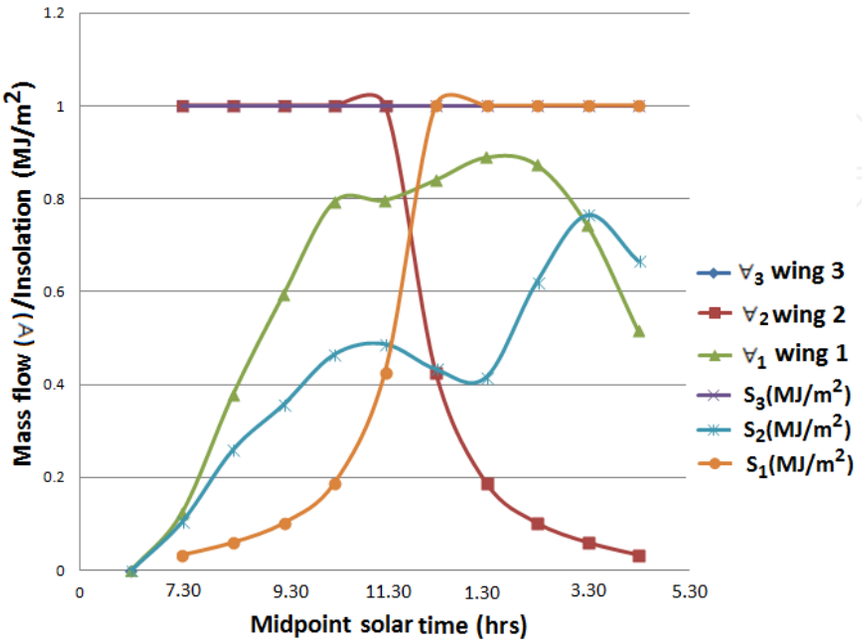

Figure 7. Graph of temperature elevation and mass flow rate and insolation

10. Conclusion

The result shows that modelling buoyant airflow within the chimney and the variation of air temperature elevation with insolation is minimal while the chimney has better efficiency at lower values of solar radiation. Thus, the method of analysis of thermal performance for this type of solar chimney has been accomplished. Nevertheless, a method of complete analytical evaluations that will give satisfactory results can be achieved by obtaining a table of correlation factor from experimental data values to analytical values of this kind.

Author details

R. S. Bello[1*], C. N. Ezebuilo[1], T. A. Adegbulugbe[2] and K. A. Eke[1]

*Address all correspondence to: segemi2002@yahoo.com

1 Federal College of Agriculture, Ishiagu, Nigeria

2 Federal College of Agriculture, Moor Plantation, Ibadan, Nigeria

References

[1] Ekechukwu, O. V. and Norton, B. (1997), "Design and measured performance of a solar chimney for natural circulation solar-energy dryers", Renewable energy, Vol. 10, pp 81-90.

[2] Mathur, J. and Mathur, S. (2006), "Summer-performance of inclined roof solar chimney for natural ventilation", Energy and Buildings, Vol. 38 No. 10, pp. 1156-1163.

[3] Bansal, N.K., Mathur, J. and Bhandari, M.S. (1993),"Solar chimney for enhanced stack ventilation", Building and Environment, Vol. 28 No. 3, pp. 373-377.

[4] Ong, K. S. (2001), A Mathematical Model of a Solar Chimney. Monash University Malaysia 46150 Petaling Jaya, Malaysia.

[5] Shiv Lal, S.C. Kaushik, P.K. Bhargav, 2013. Solar chimney: A sustainable approach for ventilation and building space conditioning. *International Journal of Development and Sustainability Online ISSN: 2168-8662 – www.isdsnet.com/ijds Volume 2 Number 1 (2013): Pages 277-297*

[6] Alter, L. (2011), "The Trombe wall: Low tech solar design makes a comeback", available at:http://www.treehugger.com/sustainable-product-design/the-trombe-wall-low-tech-solar-design-makes-a-comeback.html/ (assesses October 2012).

[7] Khedari, J. (2000), "Ventilation impact of a solar chimney on indoor temperature fluctuation and air change in a school building", Energy and Buildings, Vol. 32 No. 1, pp. 89-93.

[8] Zhai, X., Dai, Y. and Wang, R. (2005), "Comparison of heating and natural ventilation in a solar house induced by two roof solar collectors", Applied Thermal Engineering, Vol. 25 No. 5-6, pp. 741-757.

[9] Hirunlabh, J., Khedari, J. and Bunnag T. (1997), "Experimental study of a roof solar collector towards the natural ventilation of new houses", Energy and Buildings, Vol. 26 No. 2, pp. 159-164

[10] Wikipedia, 2014. Mach number. http://en.wikipedia.org/wiki/Mach_number.

[11] Onyeogu and Ibekwe, (2001). Measuring insolation data at Nsukka using a flat plate collector. Unpublished MSc thesis submitted to Dept of Mech Engr University of Nigeria Nsukka, Nigeria.

[12] Duffie, J. A. and Beckman, W. A. (2003), Solar Energy Thermal Processes. John and Sons Pub NY.

[13] Bello R. S. and Odey S. O. (2009), "Development of hot water solar oven for low temperature thermal processes", Leonardo Electronic Journal of Practices and Technologies, No. 14, 73-84 Romania. ISSN: 1583-1078 URL: www.lejpt.academicdirect.org/A14/073_084.pdf

[14] McAdams, W. H. (1954), Heat Transmission, 3rd edition, McGraw-Hill, New York.

[15] Holman J. P. (1976), Heat Transfer, National students edition, McGraw-Hill, Inc.

IntechOpen

IntechOpen